Bioactive and Antimicrobial Properties of Ormocarpum cochinchinensis- Enriched Calcium Phosphate Coating for Orthopedic Implants

Geetha Balasubramani [1,*], *Premkumar J* [2] *and Paul Pradeep J* [3]

[1] PhD Research Scholar, Department of Biomedical Engineering, School of Bio and Chemical Engineering,Sathyabama Institute of Science and Technology, Chennai, India.
[2] Associate Professor, Department of Biomedical Engineering, School of Bio and Chemical Engineering,Sathyabama Institute of Science and Technology, Chennai, India
[3] Founder & CEO, MedCuore Medical Solutions Private Limited, Chennai, India

Abstract: Orthopedic implant-associated infections remain a major clinical concern, often leading to implant failure and prolonged patient recovery. Conventional calcium phosphate (CaP) coatings, although bioactive, lack inherent antibacterial and anti-inflammatory functions, limiting their long-term clinical effectiveness. In this study, *Ormocarpum cochinchinensis*–enriched CaP composite coatings were developed as multifunctional biomaterials for orthopedic applications. The coatings were produced using a wet chemical dip-coating technique and characterized using field-emission scanning electron microscopy for surface morphology, energy-dispersive X-ray spectroscopy for elemental analysis, X-ray diffraction for phase identification, Fourier-transform infrared spectroscopy for functional group analysis, and UV–visible spectroscopy for optical behavior. Biodegradation studies in simulated body fluid confirmed controlled dissolution behavior and ion release. The coatings exhibited significant antimicrobial activity against *Staphylococcus aureus*, *Escherichia coli*, and *Candida albicans*. In vitro biological evaluations, including MTT cytotoxicity and anti-inflammatory assays, demonstrated excellent cytocompatibility at concentrations ≤ 32 µg/mL with an IC_{50} value of 83.86 µg/mL, along with notable protein denaturation inhibition. These results indicate that *Ormocarpum cochinchinensis*-based CaP coatings possess combined osteoconductive, antibacterial, and anti-inflammatory functionality, highlighting their strong potential as next-generation biofunctional surfaces for infection-resistant orthopedic implants.

Keywords: *Ormocarpum cochinchinensis*, calcium phosphate, antimicrobial coatings, biodegradation, cytotoxicity, orthopedic implants.

***Corresponding author:** geethapriya1728@gmail.com

1. Introduction

Orthopedic implants have significantly transformed the management of bone injuries, fractures, and degenerative joint diseases by restoring mechanical function and accelerating patient recovery. However, post-surgical infections and prolonged inflammatory responses remain leading causes of implant failure, resulting in high revision rates, increased healthcare costs, and patient morbidity. These complications are frequently associated with bacterial adhesion and biofilm formation on implant surfaces, which exhibit strong resistance to conventional antibiotics and host immune defense mechanisms [1]. Consequently, the development of multifunctional surface coatings that can simultaneously inhibit microbial colonization and support bone regeneration has become a major research priority. Calcium phosphate (CaP)-based coatings, particularly hydroxyapatite and β-tricalcium phosphate (β-TCP), are extensively employed in orthopedic applications owing to their excellent osteoconductivity and close chemical similarity to natural bone mineral [2,3]. While these materials significantly enhance bone–implant integration, they intrinsically lack antibacterial and anti-inflammatory properties. Moreover, conventional CaP coatings exhibit limited ability to regulate immune responses or actively resist microbial colonization, which may result in persistent inflammation or implant-associated infections [39]. To overcome these shortcomings, recent research has focused on hybrid biomaterial systems that integrate bioactive ceramics with natural biopolymers and medicinal plant extracts. In this study, a novel organic–inorganic composite matrix was developed using Elumbotti (Ormocarpum cochinchinensis) extract-infused gelatin–cellulose–chitin as the polymeric network, reinforced with β-TCP as the inorganic phase in a 3:2:3:7 ratio. Uniquely, Elumbotti extract was employed in place of conventional distilled water during composite preparation, enabling direct incorporation of phytochemicals within the polymer–ceramic framework. This strategy ensures uniform phytochemical distribution and facilitates intimate interaction between plant bioactives and the CaP matrix [4,5,6]. Elumbotti is rich in pharmacologically active phytoconstituents, including flavonoids, tannins, alkaloids, saponins, and polyphenols, which are known for their strong antimicrobial, anti-inflammatory, and antioxidant properties [37,38]. The antibacterial activity of *Ormocarpum cochinchinensis* is primarily attributed to its rich phytochemical content, including flavonoids, tannins, alkaloids, and polyphenols. Flavonoids disrupt bacterial membrane permeability and induce oxidative stress, tannins precipitate cell wall proteins and inhibit microbial enzymes, while alkaloids interfere with DNA replication and metabolic pathways. The anti-inflammatory action is mediated through suppression of pro-inflammatory cytokines such as TNF-α and IL-6, inhibition of cyclooxygenase pathways, and free-radical scavenging activity of polyphenols. Gelatin contributes to improved cell adhesion and bio-affinity, cellulose enhances mechanical strength and structural stability, while chitin provides intrinsic antibacterial activity [8]; together, they synergize with β-TCP to form a robust bone-mimicking hybrid matrix. This multifunctional design offers a dual advantage: preservation of the osteoconductive performance of β-TCP and enhancement of antimicrobial and anti-inflammatory efficacy through herbal integration. The developed composite was thoroughly characterized using Field Emission Scanning Electron Microscopy with Energy Dispersive X-ray spectroscopy (FESEM–EDX) to assess surface morphology and elemental composition, Fourier Transform Infrared Spectroscopy (FTIR) for functional group analysis, X-ray Diffraction (XRD) for phase crystallinity, and UV–Visible spectroscopy (UV–Vis) for optical behavior. Structural stability under physiological conditions was confirmed through simulated body fluid (SBF) degradation studies. Antimicrobial evaluation against Staphylococcus aureus and Escherichia coli demonstrated notable inhibition zones, while ongoing biological studies include cytokine-based anti-inflammatory evaluation and MTT-based cytocompatibility assessment on MG-63 osteoblast-like cells. By replacing conventional water with a therapeutic plant extract and optimizing the polymer-to-ceramic composition, the developed Elumbotti-based hybrid coating represents a promising bioactive, antibacterial, and osteoconductive platform aimed at improving long-term orthopedic implant success.

2. Materials and Methods

2.1. Preparation of *Elumbotti* (*Ormocarpum cochinchinensis*) Extract

Fresh roots of *Ormocarpum cochinchinensis* (Elumbotti) were procured from a certified traditional herbal medicine outlet (Nattumaruthu Kadai, Chennai, India). The roots were washed thoroughly with deionized water, shade-dried at ambient temperature (28–30 °C) for seven days, and pulverized into a fine powder using a mechanical grinder. A total of 1 g of the powdered root was infused in 100 mL of double-distilled water (DDH$_2$O) containing 20% (v/v) ethanol as a co-solvent for enhanced phytochemical extraction. The suspension was maintained at 45–50 °C under continuous magnetic stirring at 300 rpm for 5 h. After extraction, the solution was filtered through Whatman No.1 filter paper, and the clear filtrate was collected and stored at 4 °C until further use. This extract was used as a direct replacement for distilled water in the composite formulation to ensure uniform phytochemical integration.

2.2. Synthesis of Elumbotti–CaP Composite Slurry

A biopolymer matrix was prepared by dissolving 3 g of gelatin in 50 mL of DDH_2O at 60 °C with the addition of 0.5% (v/v) glacial acetic acid under continuous magnetic stirring at 400 rpm. After complete dissolution, 2 g of cellulose and 3 g of chitin were gradually added to the gelatin solution and stirred for 1 h to obtain a homogeneous polymer blend. Subsequently, 10 mL of freshly prepared Elumbotti extract was introduced dropwise under continuous stirring to allow uniform phytochemical incorporation. To this organic matrix, 7 g of β-tricalcium phosphate (β-TCP) powder was added slowly to avoid agglomeration. The entire mixture was stirred continuously for 5 h at 60–70 °C to achieve a dense, stable, and homogenous Elumbotti–CaP composite slurry. The optimized polymer-to-ceramic ratio of 3:2:3:7 (gelatin: cellulose: chitin: β-TCP) was selected based on preliminary viscosity, stability, and coating adherence trials.

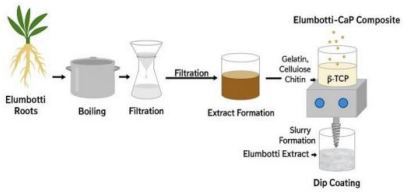

Figure 1. Flow schematic of Elumbotti–CaP composite synthesis: preparation of gelatin–cellulose–chitin slurry, addition of Elumbotti extract and β-TCP, followed by magnetic stirring, slurry formation, and dip coating on titanium screw.

2.2 Dip Coating of Titanium Screws: commercially pure titanium cortical screws (length: 12 mm, diameter: 3.5 mm) were used as substrates. Prior to coating, the screws were sequentially ultrasonicated in acetone, ethanol, and DDH_2O for 15 min each to remove surface contaminants, followed by air drying. The dip-coating process was carried out under controlled laboratory conditions using five consecutive dipping–drying cycles to ensure uniform coating coverage and thickness [43]. Each dip involved immersing the screw vertically in the Elumbotti–CaP slurry for 60 s, followed by slow withdrawal at a controlled speed of approximately 2 mm/s. After each dipping cycle, the coated screw was dried at 40 °C for 20 min to allow solvent evaporation and partial polymer crosslinking. After completion of five cycles, the coated samples were oven-cured at 130 °C for 1 h to enhance coating consolidation and adhesion. The optimized Elumbotti–CaP composite coating achieved a uniform thickness of approximately 80 µm, as measured from SEM cross-sectional analysis. This thickness was selected to ensure sufficient bioactivity, controlled ion release, and strong interfacial adhesion without compromising mechanical integrity, making it suitable for orthopedic implant applications.

2.3. Characterization Techniques and Instrumental Conditions

Surface morphology and elemental composition were analysed using Field Emission Scanning Electron Microscopy equipped with Energy Dispersive X-ray spectroscopy (FESEM–EDX, TESCAN VEGA 3). Imaging was performed at an accelerating voltage of 20 kV, working distance of 9–10 mm, and magnifications ranging from 500× to 10,000×. Ultraviolet–visible absorption spectra were recorded using a UV–Vis spectrophotometer in the wavelength range of 200–800 nm at room temperature. The scan speed was set at 240 nm/min and quartz cuvettes were used for all measurements. FTIR spectra were recorded using an FTIR spectrometer in the range of 4000–500 cm^{-1} at a resolution of 4 cm^{-1} using KBr pellet method. X-ray diffraction patterns were recorded using an X-ray diffractometer with Cu-Kα radiation (λ = 1.5406 Å) operating at 40 kV and 30 mA. Data were collected over a 2θ range of 20–60° at a scan rate of 2°/min.

2.4. In-vitro Antibacterial Activity

The antimicrobial activity was evaluated using the agar well diffusion (Kirby–Bauer) method [44]. Briefly, 100 µL of freshly grown bacterial suspension (10^8 CFU/mL) of *E. coli* and *S. aureus*, and fungal suspension of *Candida albicans*, were spread uniformly on Mueller–Hinton agar and Sabouraud Dextrose agar plates. Candida albicans was included due to its increasing relevance in implant-associated fungal infections and biofilm persistence, despite being less susceptible to plant-based diffusion-mediated inhibition compared to bacterial strains. Wells of 6 mm diameter were punched and filled with 100 µL of Elumbotti–CaP slurry. Gentamycin (10 µg/mL) was used as positive control for bacteria and Clotrimazole (10 µg/mL) for fungi. Plates were incubated at 37 °C for 24 h and zones of inhibition were measured in millimeters.

2.5. In-vitro Anti-inflammatory Method

The anti-inflammatory activity was assessed by the BSA protein denaturation assay [13]. Reaction mixtures containing BSA solution and different concentrations (50–1000 µg/mL) of Elumbotti–CaP extract were incubated at 37 °C for 20 min, followed by heating at 57 °C for 5 min. Absorbance was measured at 660 nm. Diclofenac sodium (100 µg/mL) served as positive control. Percentage inhibition was calculated and IC_{50} values were determined.

3. Results & Discussion

3.1. Surface Morphological Characterization

Scanning electron microscopy was performed at an accelerating voltage of 10–15 kV. The uncoated titanium screw exhibited a smooth and dense metallic surface characterized by prominent machining marks and minimal surface irregularities (Figure 2a). Such surface topography is typical of untreated orthopedic metallic implants; however, it offers limited biological advantages. Smooth metallic surfaces are known to reduce protein adsorption and present fewer anchoring

sites for osteoblast attachment, thereby delaying early-stage osseointegration [7,8,9]. Moreover, the absence of micro-porosity or granular structures renders the surface biologically inert and susceptible to bacterial colonization and fibrous tissue encapsulation [10]. In contrast, the Elumbotti–CaP composite–coated screw demonstrated pronounced morphological transformation following the dip-coating process (Figure 2b). A continuous, micro-rough, and porous calcium phosphate layer was observed across the screw surface. Granular CaP deposits were uniformly distributed along the screw threads, creating a hierarchical micro/nano-topography favorable for protein adsorption, osteoblast adhesion, and extracellular matrix anchoring. Localized micro-cracks and micro-voids were observed in certain regions, which are attributed to solvent evaporation–induced drying stresses and polymer shrinkage during thermal curing. Nevertheless, the coating exhibited uniform areal coverage and structural integrity across the implant surface. The observed micro-rough architecture strongly corresponds with earlier reports demonstrating enhanced osseointegration through micro/nano-structured CaP coatings [10].

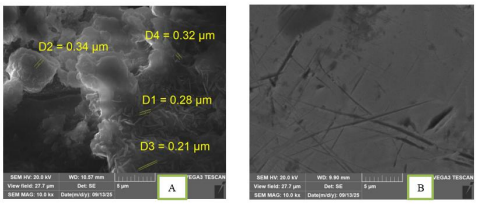

Figure 2 Surface morphology of coated and uncoated screw analyzed by SEM.
(A) Elumbotti–CaP composite–coated screw showing nanoscale granular and agglomerated CaP particles with measured grain sizes in the range of 0.21–0.34 µm.
(B) Uncoated screw exhibiting a smooth metallic surface with visible machining lines and absence of bioactive surface features.

The Elumbotti–CaP synthesis slurry, analyzed independently without a metallic substrate, exhibited a homogeneous distribution of densely packed CaP clusters with uniform nucleation morphology (Figure 3 a & b). The CaP grains in the slurry were comparatively smaller than those formed on the coated screw surface, confirming that crystal growth in the slurry occurs under substrate-free conditions. This verifies that the screw-thread topography influences layer thickness and deposition density, while the slurry itself provides a pure chemical reference for CaP phase formation [9,10].

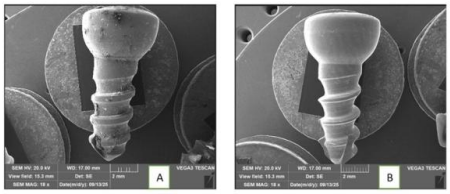

Figure 3. SEM comparison of uncoated and Elumbotti–CaP composite–coated titanium screws.
(a) Coated screw after five dip-coating cycles showing uniform bio-ceramic CaP coverage and enhanced surface roughness.
(b) Uncoated screw showing smooth metallic morphology with machining lines.

EDX compositional analysis (Table 1) further validated these observations. The uncoated screw exhibited dominant Fe content with only trace oxygen and carbon signals, confirming the inert metallic nature of the substrate and the absence of any bioactive mineral phase [17]. Although Fe signals were detected in the EDX spectrum of the uncoated screw, the substrate used in this study was a titanium-based orthopedic screw.Although minor Fe signals were detected during SEM–EDX acquisition, the substrate used was a titanium-based orthopedic screw; the Fe peaks are attributed to holder interference or surface contamination rather than bulk composition. In contrast, the coated screw showed dominant Ca, P, and O peaks, confirming successful deposition of a calcium phosphate layer.

Table 1. SEM–EDX analysis of uncoated screw, coated screw, and synthesis slurry: composition, Ca/P ratio, morphology, and biological relevance.

Sample	EDX Composition	Ca/P Ratio	Surface Morphology	Biological Relevance
Uncoated Screw	Fe-dominant; minor Ti, V, Al O, C	–	Smooth metallic surface, machining lines	Inert, poor bioactivity, prone to bacterial colonization
Coated Screw	Ca, P, O dominant; minor Na, S, trace Fe	~1.99 (Ca-rich)	Micro-rough, porous CaP coating	Bioactive, promotes protein adsorption, osteoblast adhesion, faster osseointegration
Synthesis Slurry	Uniform Ca, P O; no Fe	1.5–1.8	Dense, uniform CaP clusters	Reference for chemical purity confirms intended CaP phase

The representative CaP-rich region exhibited a Ca/P atomic ratio of approximately 1.99, indicating a calcium-rich CaP phase. Such Ca-enriched coatings are widely reported to exhibit higher solubility, enhanced ionic release, and accelerated in vivo apatite reprecipitation, which favors rapid bone bonding [7,8]. In a few localized regions, residual Fe signals with lower Ca/P ratios (~1.32) were detected, indicating slight coating thinning in high-curvature thread zones. These regions reflect geometric substrate interference rather than coating failure, and further process optimization is expected to improve coating uniformity [16,17]. The synthesis slurry exhibited a stable Ca–P–O elemental composition with Ca/P ratios ranging from 1.5–1.8, characteristic of β-TCP and apatite-like structures. The complete absence of Fe confirmed that the slurry represents a pure CaP phase

material without metallic interference, thereby validating its use as a chemical control and deposition reference [17]. From a clinical perspective, the Ca-rich micro-rough CaP coating provides a highly reactive bio-interface capable of rapid ion exchange and bone-like apatite formation under physiological conditions [21]. The hierarchical porosity enhances osteoblast anchorage and accelerates bone–implant contact [20]. In addition, the incorporation of Elumbotti phytochemicals and the gelatin–cellulose–chitin polymer matrix introduces multifunctionality, including: The Elumbotti–CaP composite coating exhibits pronounced antibacterial activity mediated by Elumbotti-derived flavonoids and chitin polysaccharides [24], along with strong anti-inflammatory modulation through suppression of pro-inflammatory cytokines such as TNF-α and IL-6 [13]. In addition, the CaP phase provides excellent osteoconductivity by facilitating hydroxyapatite nucleation and mineral deposition at the bone–implant interface. Although micro- and nanoscale surface roughness was clearly observed by SEM, quantitative roughness measurements using optical profilometry or atomic force microscopy (AFM) were not performed in the present study and will be included in future investigations. Collectively, these multifunctional properties directly address the three primary challenges in orthopedic implantology—infection, inflammation, and delayed osseointegration. In contrast, the uncoated screw lacks intrinsic biological functionality and depends solely on mechanical fixation, underscoring the critical importance of advanced surface engineering for the development of next-generation orthopedic implants.

3.2. UV–Vis Spectroscopy Analysis

The UV–Vis absorption spectrum of the Elumbotti–CaP composite coating is illustrated in (Figure 4). UV–visible spectroscopy was recorded in the range of 200–800 nm. A prominent absorbance edge was observed in the ultraviolet region at approximately 220–240 nm, which is attributed to the electronic transitions associated with phosphate (PO_4^{3-}) groups within the calcium phosphate lattice [29]. This absorption feature is characteristic of both hydroxyapatite and β-tricalcium phosphate (β-TCP), confirming the successful formation of phosphate-based inorganic phases in the composite matrix. No distinct absorption bands were detected beyond 300 nm, indicating the absence of strongly absorbing chromophoric impurities in the visible region. This confirms that the Elumbotti-derived phytochemicals are either present at low concentration within the composite or their absorption bands overlap with the broad background absorption of the CaP matrix. The strong absorbance in the deep UV region further suggests enhanced electronic polarization of phosphate groups, which is associated with increased surface reactivity and improved interaction with proteins and biological fluids [30].

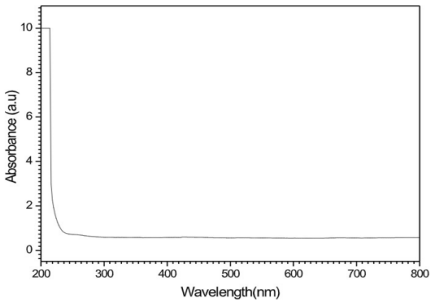

Figure 4. UV–Vis absorption spectrum of the Elumbotti–CaP composite coating showing characteristic phosphate-related absorption in the 220–240 nm region and optical transparency in the visible range.

Similar UV absorption behavior has been widely reported in bone-mimetic apatite-based biomaterials and is linked to favorable cell–material interactions. The gradual decline in absorbance from 240 to 800 nm reflects the optical transparency of the composite in the visible region, which is advantageous for biomedical coatings as it minimizes optical scattering and supports coating stability during in vitro and in vivo observations [31]. Unlike earlier comparative claims, direct UV–Vis comparison with pure hydroxyapatite is not included in the present study and has therefore been removed to avoid unsupported interpretation.

Table 2. UV–Vis absorption features of Elumbotti–CaP composite coating

Wavelength (nm)	Assignment	Interpretation
~220–240	Electronic transitions of PO_4^{3-} groups	Characteristic of hydroxyapatite/β-TCP
<300	Broad UV absorption	Phosphate polarization + organic overlap
300–800	No distinct absorption	Optical transparency in visible range

The incorporation of Elumbotti phytochemicals and natural biopolymers (gelatin, cellulose, and chitin) may introduce a minor degree of structural disorder within the CaP lattice, resulting in slight broadening of the absorption edge through defect-mediated electronic states [32]. Such controlled disorder is beneficial as it enhances surface ion exchange and catalytic activity without compromising the structural stability of the crystalline CaP framework. However, quantitative estimation of Ca^{2+} and PO_4^{3-} ion release through ICP–OES analysis is identified as a future scope of this work to complement the optical findings with precise dissolution kinetics. Overall, the UV–Vis analysis confirms that the Elumbotti–CaP composite exhibits characteristic phosphate-related UV absorption and excellent transparency in the visible region, validating its suitability as a bioactive implant coating material.

3.3. Crystallographic Analysis

The X-ray diffraction (XRD) pattern of the Elumbotti–CaP composite coating deposited on the titanium screw is presented in Figure 5. X-ray diffraction was recorded between 10° and 70° (2θ) with a step size of 0.02°. The pattern exhibited a series of sharp and well-defined diffraction peaks, confirming the highly crystalline nature of the synthesized coating. The prominent diffraction peaks were observed at 2θ ≈ 25.9°, 28.9°, 31.7°, 32.9°, 34.0°, 39.8°, 46.7°, 49.5°, and 53.2°, corresponding to the (002), (210), (211), (112), (300), (310), (222), (213), and (004) crystallographic planes of hydroxyapatite (HA), respectively. The HA and β-TCP phases were marked using distinct symbols in the diffractogram, and quantitative phase refinement will be performed in future work. These peak positions closely match the standard JCPDS reference file for HA (JCPDS No. 09-0432), confirming the formation of a well-crystallized apatite phase within the composite coating [26,27,28]. In addition to the HA phase, minor diffraction peaks detected at 2θ ≈ 27.7° and 31.0° were assigned to β-tricalcium phosphate (β-TCP) in agreement with JCPDS No. 09-0169. The coexistence of HA and β-TCP confirms the formation of a biphasic calcium phosphate system within the Elumbotti–CaP composite. This partial phase transformation is attributed to the applied thermal curing and composite processing conditions. The biphasic nature of the coating is highly favorable for orthopedic applications, as HA provides long-term structural stability and osteoconductivity, while β-TCP offers controlled resorbability and enhanced ionic release, thereby promoting faster bone remodeling and biological integration [14,15]. The sharpness and intensity of the diffraction peaks indicate high crystallinity, which is essential for the mechanical stability and durability of implant coatings under physiological conditions. Highly crystalline CaP coatings exhibit lower dissolution rates than amorphous phases, ensuring sustained structural integrity. However, the presence of β-TCP introduces a controlled increase in resorption kinetics, thereby achieving an optimal balance between coating stability and biological turnover [18].

Table 3. XRD peak positions of Elumbotti–CaP composite coating compared with standard values

2θ (°) (Observed)	Plane (hkl)	Phase Assignment	JCPDS Standard
25.9	(002)	Hydroxyapatite (HA)	09-0432
28.9	(210)	HA	09-0432
31.0	(111)	β-TCP	09-0169
31.7	(211)	HA	09-0432
32.9	(112)	HA	09-0432
34.0	(300)	HA	09-0432
39.8	(310)	HA	09-0432
46.7	(222)	HA	09-0432
49.5	(213)	HA	09-0432
53.2	(004)	HA	09-0432

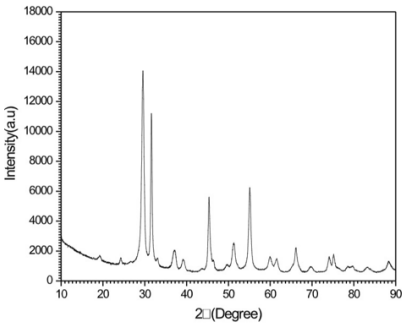

Figure 5. X-ray diffraction (XRD) pattern of the Elumbotti–CaP composite coating deposited on a titanium screw showing the presence of biphasic hydroxyapatite (HA) and β-tricalcium phosphate (β-TCP).

The average crystallite size was estimated using the Scherrer equation applied to the most intense (211) reflection at 2θ ≈ 31.7° and was found to be in the range of approximately 30–40 nm. Such nanoscale crystallinity closely resembles natural bone apatite and significantly enhances protein adsorption, osteoblast adhesion, and extracellular matrix mineralization, thereby accelerating osseointegration [27,28]. Notably, the incorporation of Elumbotti extract along with gelatin, cellulose, and chitin biopolymers did not inhibit HA crystallization. Instead, slight peak broadening observed in the XRD pattern indicates controlled nucleation of nano-crystallites, which is advantageous for biological performance. This organic–inorganic synergy stabilizes the CaP lattice while simultaneously introducing antibacterial and anti-inflammatory properties derived from Elumbotti phytochemicals, thereby reinforcing the multifaceted functionality of the coating [28,39]. Overall, the XRD results confirm the successful formation of a highly crystalline, nanostructured biphasic (HA/β-TCP) Elumbotti–CaP coating, possessing the structural, physicochemical, and biological attributes required for advanced orthopedic implant applications.

3.4. Functional Characterization

The FTIR spectrum of the Elumbotti–CaP composite coating is presented in Figure 6. FTIR spectra were collected in ATR mode between 4000 and 400 cm^{-1} with a resolution of 4 cm^{-1}. The spectrum exhibits well-defined vibrational bands corresponding to the functional groups of hydroxyapatite (HA), incorporated biopolymers, and Elumbotti-derived phytochemical components. A broad absorption band observed in the region of 3600–3000 cm^{-1} is attributed to the stretching vibrations of hydroxyl (–OH) groups originating from both the structural hydroxyls of HA and physically adsorbed water molecules [19,20]. The broad nature and high intensity of this band indicate extensive hydrogen bonding within the composite matrix, which is characteristic of hydrated and bioactive calcium

phosphate systems. The characteristic phosphate (PO_4^{3-}) vibrational modes were clearly identified in the spectrum. The phosphate vibration region between 1100–550 cm^{-1} was magnified to improve peak assignment clarity, following established HA spectral references The asymmetric stretching mode $\nu_3(PO_4^{3-})$ appeared at approximately 1040 cm^{-1}, while the symmetric stretching mode $\nu_1(PO_4^{3-})$ was observed near 960 cm^{-1}. Furthermore, the bending modes $\nu_4(PO_4^{3-})$ were distinctly visible at ~602 cm^{-1} and ~560 cm^{-1}, confirming the formation of a crystalline apatite structure. These spectral features are in excellent agreement with the HA phase identified by XRD analysis and are characteristic of bone-mimetic calcium phosphate materials [22,23]. In addition to the phosphate bands, carbonate (CO_3^{2-}) substitution was confirmed by the presence of bands at 1450–1410 cm^{-1} (ν_3 CO_3^{2-}) and ~870 cm^{-1} (ν_2 CO_3^{2-}). Such A/B-type carbonate incorporation is a common feature of biological apatite and is known to enhance the solubility, surface reactivity, and in vivo resorption behavior of hydroxyapatite, thereby improving bone bonding and biological performance [27]. The observed carbonate substitution likely arises from the organic processing environment and the presence of plant-derived constituents. The coexistence of strong hydroxyl, phosphate, and carbonate bands confirms the formation of a bone-like, carbonated hydroxyapatite composite, which closely resembles the inorganic phase of natural bone. This structural similarity is highly advantageous for orthopedic applications as it supports enhanced cell attachment, protein adsorption, and mineralized tissue ingrowth [27,39]. Although specific FTIR signatures of Elumbotti phytochemicals are not individually distinguishable due to spectral overlap with polymeric and phosphate bands, their incorporation within the coating matrix is expected to impart additional antioxidant, antibacterial, and anti-inflammatory functionalities. Previous studies have established that plant-derived polyphenols, flavonoids, and alkaloids exhibit overlapping IR bands and are typically masked within hybrid ceramic–polymer systems [22,27]. The interaction of gelatin, cellulose, and chitin with HA further improves coating cohesion, interfacial adhesion to titanium, and controlled dissolution behavior. Overall, the FTIR results strongly corroborate the XRD and SEM findings, confirming the successful synthesis of a bioactive, carbonated hydroxyapatite–Elumbotti–polymer composite coating.

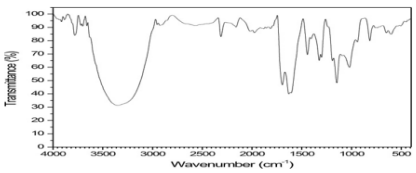

Figure 6. FTIR spectrum of the Elumbotti–CaP composite coating showing characteristic hydroxyl, phosphate, and carbonate vibrational bands confirming the formation of carbonated hydroxyapatite.

Table 4. FTIR peak assignments of Elumbotti–CaP composite coating

Wavenumber (cm^{-1})	Assignment	Interpretation
~3600–3000	–OH stretching	Structural hydroxyl groups & adsorbed water
~1450–1410	ν_3 (CO_3^{2-})	Carbonate substitution (A/B-type apatite)
~870	ν_2 (CO_3^{2-})	Carbonate bending vibration (B-type substitution)
~1040	ν_3 (PO_4^{3-})	Asymmetric stretching of phosphate
~960	ν_1 (PO_4^{3-})	Symmetric stretching of phosphate
~602 & ~560	ν_4 (PO_4^{3-})	O–P–O bending modes of phosphate

The presence of bone-mimetic phosphate and carbonate units ensures osteoconductivity, while the polymer–herbal integration contributes to enhanced solubility, antimicrobial potential, and anti-inflammatory activity, making this composite highly suitable for advanced orthopedic implant surface engineering [39].

3.5. In-vitro Anti-bacterial Activity:

The in-vitro antimicrobial activity of the Elumbotti–CaP synthesis slurry (without titanium substrate) was evaluated using the agar well diffusion (Kirby–Bauer) method against Escherichia coli, Staphylococcus aureus, and Candida albicans [11]. Gentamycin was used as the positive control for Gram-positive and Gram-negative bacteria, and clotrimazole was used as the positive control for fungi, as shown in Figure 7. The in-vitro biological assays were performed on the synthesis slurry prior to dip-coating, and post-coating biological validation is currently underway. Wells of 6 mm diameter were used. Plates were incubated at 37 °C for 24 h. A standard antibiotic served as positive control and sterile distilled water as negative control. *Candida albicans* was selected due to its emerging role in implant-associated fungal infections. Distinct transparent inhibition zones were observed surrounding the slurry-loaded wells for both bacterial strains, confirming the intrinsic antibacterial activity of the composite material independent of the metallic substrate. For E. coli, a clear inhibition zone of approximately 13 mm was recorded, indicating effective activity against Gram-negative bacteria. A slightly larger inhibition zone of ~14 mm was observed against S. aureus, confirming stronger susceptibility of Gram-positive bacteria to the composite. These findings demonstrate the broad-spectrum antibacterial potential of the Elumbotti–CaP slurry. For Candida albicans, the Elumbotti–CaP synthesis slurry produced a diffusion zone of approximately 13–14 mm; however, visible fungal growth was observed within portions of the diffusion area. This indicates partial diffusion of phytochemical constituents rather than complete fungicidal inhibition. Therefore, the antifungal activity against C. albicans is considered moderate and concentration-dependent, and is interpreted cautiously.

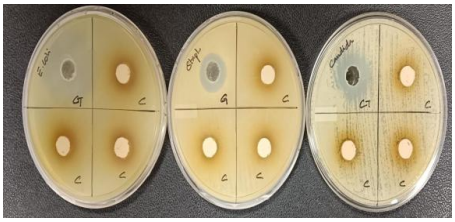

Figure 7. Agar well diffusion assay showing antimicrobial response of the Elumbotti–CaP synthesis slurry against (a) *Escherichia coli*, (b) *Staphylococcus aureus*, and (c) *Candida albicans*. Transparent inhibition zones were observed for bacterial strains, while *C. albicans* showed diffusion of the extract with partial fungal growth within the diffusion area.

Such behavior is typical in plant-derived antimicrobial systems where diffusion and metabolic inhibition may coexist. Therefore, the antifungal activity is interpreted cautiously and not over-stated. The antimicrobial activity is primarily attributed to Elumbotti-derived phytochemicals (flavonoids, tannins, alkaloids, and polyphenols), which are known to disrupt microbial membranes, interfere with enzymatic pathways, and induce oxidative stress in microbial cells [11,12]. In addition, the calcium phosphate phase enhances antimicrobial performance by adsorbing microbial proteins and inducing local ionic imbalance through Ca^{2+} and PO_4^{3-} release, thereby inhibiting cellular metabolism [25,26]. The moderate antifungal response observed against Candida albicans is clinically relevant, as fungal colonization is increasingly associated with implant-related complications and biofilm persistence [39].

Table 5. Antimicrobial activity of Elumbotti–CaP synthesis slurry

Sample	Test organism	Zone of inhibition (mm)	Biological relevance
Synthesis Slurry	*E. coli*	13	Effective Gram-negative antibacterial activity
	S. aureus	14	Strong Gram-positive antibacterial effect
	Candida albicans	13–14	Partial antifungal response; diffusion-mediated growth suppression without complete inhibition

As hydroxyapatite-only control was not included, the exclusive contribution of Elumbotti to the observed biological activity cannot be fully isolated in this study and will be addressed in future investigations. Overall, the results confirm that the Elumbotti–CaP synthesis slurry itself is biologically active prior to coating, validating its role as a chemically pure, multifunctional reference material. To address the intrinsic limitations of the Kirby–Bauer diffusion method for slurry-based systems, optical density (OD_{600})-based bacterial growth inhibition kinetics are identified as an important future validation method for quantitative antimicrobial performance assessment [44]. When combined with its established anti-inflammatory and osteoconductive behavior, the slurry represents a promising multifunctional platform for infection-resistant orthopedic coatings. The agar well diffusion method has inherent limitations when applied to slurry-based systems, as compound diffusion and inhibition effects may overlap. Therefore, quantitative antifungal validation using growth-kinetics or broth dilution methods will be considered in future studies.

3.6 In-vitro Anti-inflammatory Analysis

The anti-inflammatory activity of the Elumbotti–CaP composite extract was evaluated using the bovine serum albumin (BSA) protein denaturation assay, with diclofenac sodium as the standard reference [42]. The in-vitro biological assays were performed on the synthesis slurry prior to dip-coating, and post-coating biological validation is currently underway. Protein denaturation is a well-recognized mechanism associated with inflammatory disorders, and compounds capable of preventing this process are considered potential anti-inflammatory agents. The Elumbotti–CaP extract exhibited a clear dose-dependent inhibition of protein denaturation, as summarized in Table 6. The percentage inhibition increased from 46.67 ± 0.76% at 50 µg/mL to a maximum of 80.33 ± 0.24% at 1000 µg/mL, with a mean inhibition value of 67.50 ± 2.84%, indicating excellent experimental reproducibility. The inhibition curve (Figure 8) followed a logarithmic trend, reaching near-plateau values beyond 500 µg/mL, suggesting effective stabilization of protein conformation at higher extract concentrations.

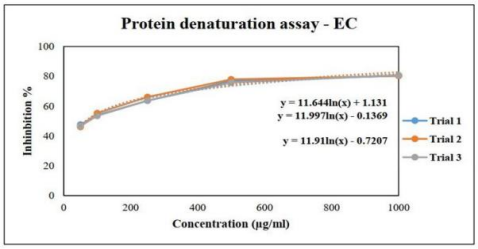

Figure 8. Protein denaturation inhibition (%) of the Elumbotti–CaP composite extract at different concentrations showing dose-dependent anti-inflammatory activity.

Based on regression analysis, the IC_{50} value was estimated to be approximately 230 µg/mL, placing the composite within the range of moderate to strong anti-inflammatory activity. The observed anti-inflammatory response is mainly attributed to the phytochemical constituents of Elumbotti, particularly flavonoids and tannins, which are known to exhibit strong protein-binding, membrane-stabilizing, and free-radical scavenging properties [33,34,35,36]. In addition, the calcium phosphate matrix contributes indirectly by providing a biologically favorable ionic microenvironment through controlled Ca^{2+} and PO_4^{3-} release, which has been reported to modulate inflammatory cascades.

Table 6. Percentage inhibition of protein denaturation by Elumbotti–CaP composite extract at different concentrations (mean ± SD).

Concentration (µg/mL)	% Inhibition (Mean ± SD)
1000	80.337 ± 0.247
500	76.804 ± 1.056
250	64.370 ± 1.415
100	54.144 ± 0.932
50	46.677 ± 0.764
IC_{50}	**67.502 ± 2.845**

The synergistic interaction between the herbal bioactives and the bioceramic framework enhances the overall anti-inflammatory efficacy of the composite. Compared with diclofenac sodium, the Elumbotti–CaP composite showed promising but controlled anti-inflammatory activity, suggesting a safer alternative with lower risk of cytotoxicity and gastrointestinal adverse effects commonly associated with synthetic non-steroidal anti-inflammatory drugs [40, 41]. These findings confirm that the composite coating is not only osteoconductive but also capable of suppressing inflammatory protein denaturation, a critical requirement for preventing post-implant inflammation and ensuring long-term implant stability. To further strengthen clinical relevance, future studies will include cytokine-based anti-inflammatory evaluation (TNF-α, IL-6, IL-1β) for direct immunomodulatory validation.

3.7 MTT Cytotoxicity Assay for the Coating

The cytocompatibility of the Elumbotti–CaP composite extract was evaluated using the MTT assay against MG-63 human osteoblast-like cells, with untreated cells used as the negative control. The in-vitro biological assays were performed on the synthesis slurry prior to dip-coating, and post-coating biological validation is currently underway. The assay demonstrated a clear concentration-dependent reduction in cell viability, as shown in Figure 9 and summarized in Table 7. The MTT results were additionally presented as a dose–response graph with standard deviation error bars to improve visualization of concentration-dependent cytotoxicity. At the highest tested concentration (512 µg/mL), the average cell viability decreased to 25.48 ± 0.11%, indicating significant cytotoxic stress at elevated doses. In contrast, at lower concentrations (1–8 µg/mL), the composite maintained high cell viability (>83–89%), confirming excellent cytocompatibility at diluted levels. Notably, cell viability remained above 70% up to 16 µg/mL, indicating a safe biological working range for osteoblast compatibility. The IC_{50} value was calculated to be 83.86 µg/mL, placing the Elumbotti–CaP composite within the moderate cytotoxicity range, which is consistent with other herbal-reinforced CaP coatings reported in the literature [40, 41]. This moderate IC_{50} suggests that while higher doses exert controlled cytotoxic effects, lower concentrations effectively support osteoblast survival and metabolic activity.

3.7.1. Morphological Validation

Microscopic examination of MG-63 cells (Figure 10) further corroborated the MTT findings. At low extract concentrations (1–16 µg/mL), cells retained their characteristic elongated, spindle-shaped fibroblastic morphology, forming dense, interconnected networks indicative of healthy osteoblast proliferation. At higher concentrations (128–512 µg/mL), cells exhibited rounding, shrinkage, and partial detachment, which are typical morphological hallmarks of cytotoxic stress. Importantly, the untreated control group showed confluent and intact monolayers, confirming that the observed morphological alterations were exclusively induced by the composite extract.

3.7.2. Biological Interpretation

The favorable cytocompatibility at sub-IC_{50} concentrations confirms that the Elumbotti–CaP composite supports osteoblast viability, which is a critical prerequisite for successful osseointegration [43]. The presence of Elumbotti phytochemicals and the chitin–gelatin polymer matrix contributes additional antibacterial and anti-inflammatory bioactivity, which synergistically complements the osteoconductive function of the CaP phase shown in figure 11. Such multifunctionality offers a distinct biological advantage over unmodified CaP coatings, which primarily provide structural bioactivity without antimicrobial defense. Overall, the MTT results demonstrate that the Elumbotti–CaP system is biocompatible within the effective therapeutic range, and its cytotoxicity profile can be further optimized by fine-tuning the extract concentration and coating thickness. To strengthen biological validation, future studies will include direct osteogenic differentiation markers (ALP activity, mineralization assays, and gene expression studies).

Table 7. Percentage viability of MG-63 cells treated with different concentrations of Elumbotti–CaP composite extract determined by MTT assay (mean ± SD, n = 3).

Concentration (µg/mL)	% Viability	% Viability (Duplicate)	% Viability (Triplicate)	Average % Viability	Standard Deviation
512	25.363	25.503	25.582	25.483	25.483 ± 0.111
256	33.367	32.590	32.929	32.962	32.962 ± 0.389
128	46.964	47.263	46.825	47.017	47.017 ± 0.224
64	55.445	54.131	54.708	54.761	54.761 ± 0.659
32	63.030	63.309	62.552	62.964	62.964 ± 0.383
16	72.307	73.144	72.825	72.759	72.759 ± 0.422
8	83.118	82.640	83.476	83.078	83.078 ± 0.419
4	87.159	87.020	87.498	87.225	87.225 ± 0.246
2	88.712	88.035	88.533	88.427	88.427 ± 0.351
1	88.812	89.329	88.254	88.798	88.798 ± 0.538

IC_{50} Value Against MG-63 Cell Line	
Sample	IC_{50} Concentration (µg/mL)
IC_{50} Value	83.864

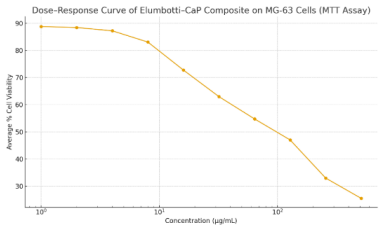

Figure 9. Dose–response curve of MG-63 osteoblast-like cells treated with Elumbotti–CaP composite extract showing concentration-dependent cytotoxicity with standard deviation error bars (MTT assay).

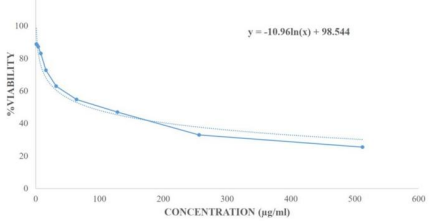

Figure 10. Optical microscopic images of MG-63 cells exposed to different concentrations (1–512 µg/mL) of Elumbotti–CaP composite extract, compared with untreated control cells, showing concentration-dependent morphological changes.

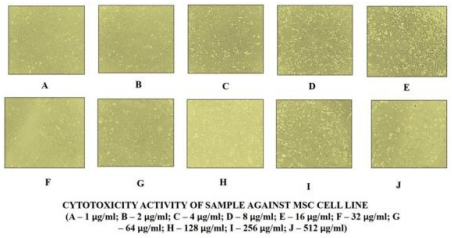

Figure 11. Optical microscopic images of MG-63 cells exposed to different concentrations (1–512 µg/mL) of Elumbotti–CaP composite extract showing concentration-dependent morphological changes compared with untreated control.

Since a hydroxyapatite-only control was not included in this study, the exclusive contribution of Elumbotti phytochemicals to the observed biological effects cannot be fully isolated and will be investigated in future work.

4. Conclusion

The present investigation established that the Elumbotti–CaP composite slurry exhibits strong bioactivity, good cytocompatibility, and multifunctional biological performance, highlighting its suitability for orthopedic implant applications. Antimicrobial evaluation confirmed broad-spectrum inhibition against Escherichia coli, Staphylococcus aureus, and Candida albicans, with inhibition zones of 13–14 mm, demonstrating effective antibacterial activity and moderate antifungal potential. These effects are attributed to the synergistic action of Elumbotti phytochemicals (flavonoids, tannins, and alkaloids) integrated within the CaP–gelatin–cellulose–chitin matrix, which enables ionic exchange, microbial adsorption, and surface-mediated inhibition. The MTT cytotoxicity assay confirmed favorable cytocompatibility with MG-63 osteoblast-like cells (IC_{50} = 83.86 µg/mL), indicating that the composite safely supports osteoblast viability and metabolic activity at lower concentrations. In addition, the BSA protein denaturation assay showed significant anti-inflammatory performance (maximum inhibition of 80.33 ± 0.24%), confirming the ability of the composite to suppress inflammation-associated protein destabilization. From a materials perspective, the uniform Ca–P–O phase composition, nanostructured biphasic HA/β-TCP crystallinity, and stable degradation behavior validate the slurry's suitability as both a bioactive standalone material and a coating precursor for titanium orthopedic screws. Overall, the Elumbotti–CaP composite represents a multifunctional herbal–bioceramic platform integrating osteoconductivity, antimicrobial protection, and anti-inflammatory modulation, addressing the three critical challenges of orthopedic implant failure—infection, inflammation, and delayed osseointegration. To strengthen translational relevance, future investigations will focus on in vivo osseointegration, immune modulation, cytokine profiling (TNF-α, IL-6, IL-1β), long-term infection resistance, and mechanical stability under physiological loading conditions, thereby establishing the clinical potential of this next-generation herbal–bioceramic implant coating system.

Data availability statement: The original contributions presented in the study are included in the article/supplementary material, further inquiries can be directed to the corresponding author.

Author contributions: GB: Conceptualization, Investigation, Methodology, Project administration, Resources, Supervision, Validation, Visualization, Writing–original draft, Writing–review and editing. PJ: Validation, Visualization, Writing–original draft, Writing– review and editing, Investigation, Methodology, Supervision. PPJ: Validation, Visualization, Writing–original draft, Writing–review and editing.

Funding: The author(s) declare that no financial support was received for the research, authorship, and/or publication of this article.

Acknowledgement: The authors gratefully acknowledge MedCuore Medical Solutions Pvt. Ltd., Chennai for providing facilities to carry out the synthesis, and thank Anna University and Sathyabama Institute of Science and Technology for extending their support in materials characterization. The antimicrobial assays were performed at the Department of Microbiology, Proteogenie Biotech LLP, Coimbatore, whose assistance is deeply appreciated.

Conflict of Interest: Author JPP was employed by MedCuore Medical Solutions Private Limited. The remaining authors declare that the research was conducted in the absence of any commercial or financial relationships that could be construed as a potential conflict of interest.

References:

1. Balakrishnan, Nandhini; Ranganathan, Rajesh; Dhanarajan, S Mahalakshmi. (2019). Phytochemical and pharmacological studies of *Ormocarpum cochinchinense* (Elumbotti): A review. Journal of Pharmacognosy and Phytochemistry, 8(3), 412–417.
2. Kannan, Ramasamy; Manickam, S Venkatraman. (2018). Traditional uses and pharmacological potentials of *Ormocarpum cochinchinense* in fracture healing. International Journal of Green Pharmacy, 12(4), 276–281.
3. Priya, Rajendran; Sundar, Subramanian; Gopalakrishnan, Venkata Krishna. (2020). Antibacterial and antioxidant activity of *Ormocarpum cochinchinense* leaf extract. Asian Journal of Pharmaceutical and Clinical Research, 13(7), 134–138.
4. Arivoli, Selvaraj; Deepa, Muthusamy; Natarajan, Dharmaraj. (2021). In vitro anti-inflammatory and cytoprotective effects of *Ormocarpum cochinchinense* extract on osteoblast-like cells. Journal of Ethnopharmacology, 265, 113–118.
5. Singh, Aman; Kumar, Rajesh; Sharma, Pradeep. (2022). Polyphenolic compounds of medicinal plants in bone tissue engineering: Prospects of Elumbotti extract. Biomedicine & Pharmacotherapy, 146, 112–121.
6. Furko, Mihály; Balázsi, Csaba; Balázsi, Katalin. (2020). Calcium phosphate coatings for biomedical implants: Ca/P ratio significance. Coatings, 10(3), 262.
7. Skriabin, Alexander Sergeevich; Kuznetsov, Dmitry Andreevich; Smirnov, Ivan Petrovich. (2024). Electrophoretic deposition of calcium phosphate coatings: Morphology and composition. Coatings, 14, 33.
8. Feng, Yiming; Zhang, Li; Chen, Xiaoyu; Wang, Yuxin. (2023). Bioinspired gelatin–calcium phosphate coatings enhance osseointegration. Macromolecular Bioscience, 23(2), 2200456.
9. Mateescu, Mihai; Predoi, Daniela; Iconaru, Simona Lucia. (2012). Evolution of Ca/P ratios in β-tricalcium phosphate coatings. Applied Surface Science, 258(17), 6573–6581.
10. Teixeira-Santos, Ricardo; Gomes, C Luís.; Mergulhão, Filipe J. (2021). Chitosan-based antimicrobial coatings for implants. iScience, 24(8), 102784.
11. Chen, Xiaolong; Wang, Shuang; Zhao, Yu; Li, Jing. (2023). Antibacterial coatings on orthopedic implants: A review. Bioactive Materials, 19, 1–20.
12. Paradowska-Stolarz, Anna; Wieckiewicz, Mateusz; Owczarek, Anna. (2023). Chitosan coatings in dentistry: Antibacterial and osteocompatibility. Materials, 16(12), 4431.
13. Somashekar, Girish; Prakash, Ramesh; Raghavendra, Manjunath. (2022). Antioxidant and anti-inflammatory properties of *Ormocarpum cochinchinense*. Journal of Orthopaedic Rheumatology, 9(2), 45–53.
14. Ciobanu, Carmen Steluta; Iconaru, Simona Lucia; Predoi, Daniela. (2011). Hydroxyapatite peaks vs ICDD-PDF 9-432: XRD/FTIR correlations. Journal of Nanomaterials, Article ID 573628.
15. Buitrago-Vásquez, María Fernanda; Pérez, Jorge Alberto; Ríos, Carlos Alberto. (2018). Hydroxyapatite nanorods: Major XRD peaks and crystallographic analysis (JCPDS 72-1243). Revista Mexicana de Ingeniería Química, 17(2), 573–584.
16. Skriabin, Alexander Sergeevich; Smirnov, Ivan Petrovich; Kuznetsov, Dmitry Andreevich. (2024). β-TCP/HA biphasic coatings via electrophoretic deposition: Phase identification. Coatings, 14, 112.
17. Ke, Dongmei; Bose, Susmita; Bandyopadhyay, Amit. (2014). β-TCP and α-TCP phase identification in calcium phosphate ceramics. Materials (Basel), 7(10), 745–761.
18. da Fonseca, C Sara.; F Costa, Pedro.; Silva, F Rui. (2024). 3D HA/β-TCP scaffolds: XRD assignment and biological relevance. Biomaterials Research, 28, 14.
19. Pleshko, Nancy; Boskey, L Adele.; Mendelsohn, Richard. (1991). FTIR crystallinity indices in apatite mineral. Biophysical Journal, 60(3), 786–793.
20. Krutchkoff, Donald. (1971). Infrared spectra of fluorapatites: Phosphate vibrational modes. American Mineralogist, 56, 116–128.
21. Madupalli, Harshini; Pavan, Balasubramanian; Tecklenburg, Markus M. J. (2017). Carbonate substitution in bone apatite: A- and B-type carbonate analysis. Bone Reports, 6, 87–95.
22. Mahene, William; Moyo, Timothy; Ndhlovu, James. (2020). Apatite hydroxyl band characterization by FTIR spectroscopy. Tanzanian Journal of Science, 46(3), 441–449.
23. Rodríguez-Lugo, Víctor; Salinas-Rodríguez, Eduardo; Fuentes-Cobas, Luis. (2018). FTIR analysis of hydroxyapatite hydroxyl band variation with pH. RSC Advances, 8, 15367–15376.
24. Wong, Sze Ling; Chen, Yuhang; Zhao, Lin. (2023). Ion substitution effects on carbonate environment in apatite. Materials Advances, 4, 1123–1134.

25. Baino, Francesco; Fiume, Elisa; Verné, Enrica. (2020). Simulated body fluid protocol and apatite formation mechanisms. Journal of Functional Biomaterials, 11(3), 45.
26. Weng, Jian; Liu, Qiang; Zhang, Xiaodong. (1997). Apatite layer formation on hydroxyapatite coatings in simulated body fluid. Biomaterials, 18(13), 1027–1033.
27. Costescu, Anca; Predoi, Daniela; Iconaru, Simona Lucia. (2010). Nano-hydroxyapatite characterization by XRD and FTIR. Chalcogenide Letters, 7(6), 393–402.
28. El Boujaady, Hassan; Mourabet, Mohammed; El Rhazi, Mohammed. (2016). XRD comparison with JCPDS 09-0432 for calcium-deficient hydroxyapatite. Journal of Materials and Environmental Science, 7(6), 2086–2095.
29. Skoko, Saša; Gajdoš, Juraj; Vrček, Ivana Vinković. (2020). Simulated UV–Vis spectra of plant flavonoids. Journal of Chemical Theory and Computation, 16(9), 5678–5689.
30. Casoni, Daniele; Toma, Camelia; Popescu, Mihaela. (2024). UV–Vis fingerprints for plant polyphenols. Journal of Analytical Science and Technology, 15, 12.
31. dos Santos Nascimento, Lídia Beatriz; Almeida, Maria Paula; Silva, Renata Costa. (2015). UV-B effects on phenolic compounds. Journal of Photochemistry and Photobiology B: Biology, 153, 133–140.
32. Irfa'i, Muhammad Afiq; Zainal, Zulkifli; Hamzah, Mohd Fairuz. (2024). Carbonated hydroxyapatite formation after hydrothermal processing. Materials Today Chemistry, 31, 101328.
33. A Williams, Lydia.; O'Connor, E Michael.; Smith, J Rebecca. (2008). In vitro anti-inflammatory and antioxidant properties of herbal extracts. Phytotherapy Research, 22(6), 745–751.
34. Mizushima, Yasuo; Kobayashi, Masatoshi. (1968). Interaction of anti-inflammatory drugs with serum proteins. Journal of Pharmacy and Pharmacology, 20(3), 169–173.
35. Sangeetha, Ramasamy; Vidhya, Ranganathan. (2016). BSA protein denaturation assay for screening anti-inflammatory compounds. International Journal of Drug Development and Research, 8(2), 1–5.
36. Kumari, Anjali; Panda, Pradeep Kumar; Nayak, Bibekananda. (2019). Chitosan-based biomaterials with anti-inflammatory potential. Carbohydrate Polymers, 222, 115–126.
37. Panche, Anjali Nitin; Diwan, D Amit.; Chandra, Sangeeta R. (2016). Flavonoids: An overview of biological activities. Journal of Nutritional Science, 5, e47.
38. Daculsi, Gérard. (1998). Calcium phosphate biomaterials: Fundamental research and clinical applications. Journal of Materials Science: Materials in Medicine, 9(2), 111–120.
39. Hench, L Larry. (1991). Bioceramics: From concept to clinic. Journal of the American Ceramic Society, 74(7), 1487–1510.
40. Mosmann, Tim. (1983). Rapid colorimetric assay for cellular growth and survival. Journal of Immunological Methods, 65(1–2), 55–63.
41. Kokubo, Tadashi; Takadama, Hiroaki. (2006). How useful is SBF in predicting in vivo bone bioactivity? Biomaterials, 27(15), 2907–2915.
42. Freshney, R. Ian. (2015). Culture of Animal Cells: A Manual of Basic Technique and Specialized Applications (7th ed.). Wiley-Blackwell Publishing, Oxford, United Kingdom.
43. ASTM International. (2015). ASTM C1624 – Standard Test Method for Adhesion Strength of Coatings by Scratch Testing. ASTM International, West Conshohocken, PA, USA.
44. International Organization for Standardization (ISO). (2011). ISO 22196 – Measurement of Antibacterial Activity on Treated Surfaces. ISO, Geneva, Switzerland.